ACS Catalysis

Research Article

pubs.acs.org/acscatalysis

N-Doping-Induced Nonradical Reaction on Single-Walled Carbon Nanotubes for Catalytic Phenol Oxidation

Xiaoguang Duan, Hongqi Sun,* Yuxian Wang, Jian Kang, and Shaobin Wang*

Department of Chemical Engineering, Curtin University, GPO Box U1987, Perth, Western Australia 6845, Australia

Supporting Information

ABSTRACT: Metal-free materials have been demonstrated to be promising alternatives to conventional metal-based catalysts. Catalysis on nanocarbons comparable to that of cobalt- or manganese-based catalysts in peroxymonosulfate (PMS) activation has been achieved, yet the catalyst stability has to be addressed and the mechanism also needs to be elucidated. In this study, N-doped carbon nanotubes (NoCNTs) were employed as metal-free catalysts for phenol catalytic oxidation with sulfate radicals and, more importantly, a detailed mechanism of PMS activation and the roles of nitrogen heteroatoms were comprehensively investigated. For the first time, a nonradical pathway accompanied by radical generation ($^{\bullet}OH$ and $SO_4^{\bullet-}$) in phenol oxidation with PMS was discovered upon nitrogen heteroatom doping. The NoCNTs presented excellent stability due to the emerging nonradical processes. The findings can be used for the design of efficient and robust metal-free catalysts with both superior catalytic performance and high stability for various heterogeneous catalytic processes.

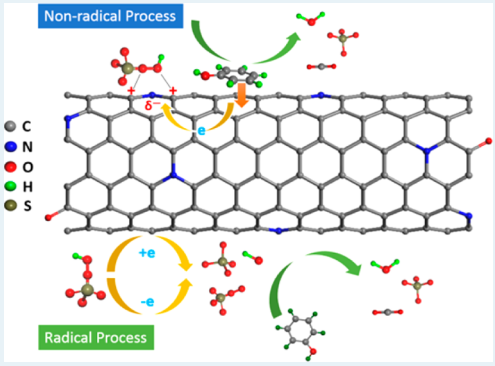

KEYWORDS: *metal-free catalysis, carbon nanotubes, nitrogen doping, nonradical, sulfate radicals*

INTRODUCTION

Modern chemistry and chemical engineering rely heavily on catalytic processes that have dramatically initiated and sustained global industrialization.[1] Most homogeneous and heterogeneous catalytic processes are based on either noble,[2] transition,[3] and rare-earth[4] metals or their oxides. The issues of metal-based catalysts, such as their scarcity in nature, deactivation, high cost in disposal of waste catalysts, and secondary pollution, have been experienced in terms of sustainable development. Moreover, the inherent chemical complexity of metal-based catalysts, including various forms of polyvalent states,[5] bridging and terminal lattice oxygens,[6] and side reactions,[7] has imposed a variety of difficulties in mechanistic studies.[1,8] Therefore, novel metal-free materials are highly desirable as alternatives to metal-based catalysts.

In environmental remediation, advanced oxidation processes (AOPs) have been widely employed, owing to the complete destruction of organic pollutants to give water and carbon dioxide.[9] Most AOPs such as the Fenton reaction,[10] catalytic ozonation,[11] photocatalysis,[12] and oxidation with sulfate radicals[13,14] are based on catalytic processes. In most cases, metal-based catalysts were used to mediate the formation of reactive radicals. Hydroxyl radicals ($^{\bullet}OH$) have been observed in most of the above AOPs and demonstrated high efficiencies and almost no selectivity to organic pollutants. The demerits of hydroxyl radicals are the low pH of 3−4 (Fenton), use of specific instruments (ozonation and photocatalysis), and secondary contamination of sludge and metal leaching.[15]

In 1956, Ball and Edward[16] discovered that peroxymonosulfuric acid (Caro's acid) was highly reactive and able to facilitate degradation of pollutants in water. The involved sulfate radicals not only are flexible to a wide pH range up to neutral and basic conditions but also have a higher redox potential of 2.5−3.1 V than the 1.8−2.7 V of hydroxyl radicals, indicating a more powerful oxidation capability.[17,18] Homogeneous metal ions[13,14] and heterogeneous metal oxides[5,15,19,20] have been recently applied to activate peroxymonosulfate (PMS) to generate sulfate radicals for the decomposition of organic pollutants. The main problem of these catalytic oxidation processes was toxic metal leaching.

Recently, metal-free materials have attracted increasing attention as sustainable alternatives to metal-based catalysts. In energy conversion or chemical synthesis, metal-free catalysts are expected to reduce the cost, prevent deactivation, and facilitate mechanistic studies.[21−23] For environmental catalysis, metal-free catalysts can provide an extra advantage of nonsecondary contamination, especially in water remediation. For the first time, we reported that chemically reduced graphene oxide (rGO) is able to activate PMS to produce sulfate radicals for phenol oxidation.[24] Physical and chemical modifications were able to create porous structures, tune the surface acidity/alkalinity, and then improve the adsorption and catalytic activity of rGO.[25,26] Further studies also suggested that nitrogen doping can significantly enhance the efficiencies of nanocarbons in PMS activation.[27,28] Though oxygen functional groups, defective edges, and heteroatoms in the sp^2 carbon

Received: November 7, 2014
Revised: December 3, 2014
Published: December 10, 2014

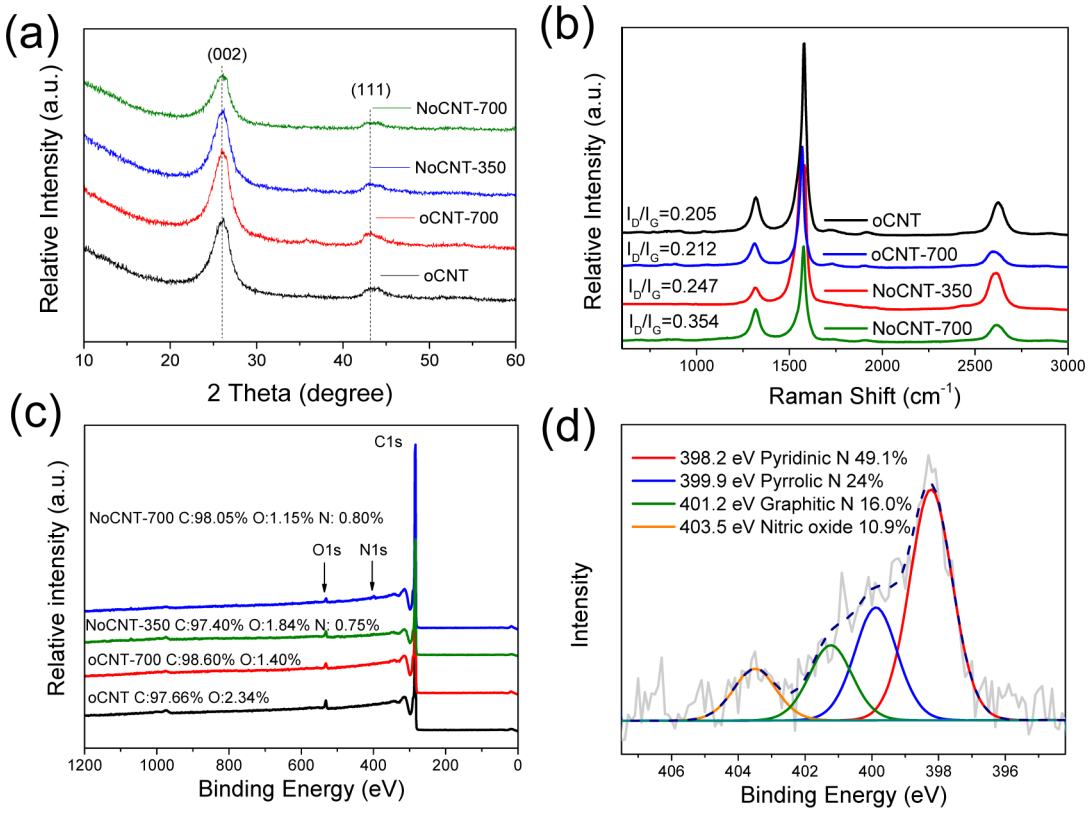

Figure 1. (a) XRD patterns of oCNT, oCNT-700, NoCNT-350, and NoCNT-700, (b) Raman spectra of CNTs samples, (c) XPS survey of CNTs samples, (d) N 1s spectra of NoCNT-700.

framework were suggested to be the active sites, a solid and insightful mechanism of PMS activation on nanocarbons is still lacking. Moreover, the stability of metal-free materials is required to enable practical applications.

In this study, we developed a one-pot synthesis of N-doped nanocarbon (NoCNT-700) using single-walled carbon nanotubes (oCNTs) with a novel N precursor of melamine at 700 °C. This synthesis was free of critical conditions such as vacuum, plasma, and high temperature above 900 °C and toxic/explosive nitrogen precursors such as NH_3 and ammonium nitrate.[27−29] The high degree of graphitic structure and low oxygen content in CNTs would make it possible to identify the roles of doped nitrogen. Electron paramagnetic resonance (EPR) and classical radical quenching tests were used to investigate the PMS activation and phenol oxidation. Unlike the case for other AOPs in which free radicals are the keys for organic degradation, nonradical processes were, for the first time, observed on the modified CNT samples upon nitrogen doping. Nonradical processes were identified in Fenton or Gif chemistry (selective hydrocarbon activation chemistry)[30−32] yet have been barely reported in AOPs. Very recently, Zhang et al.[33,34] indicated that ozonation or peroxydisulfate (PDS) activation without radical generation can degrade organic pollutants in water. CuO was essential in ozonation and PDS activation. Nevertheless, nonradical oxidation has never been reported in carbocatalysis for heterogeneous oxidation. The observation of nonradical processes of PMS activation upon nitrogen doping in this study significantly contributed to mechanistic studies on the active sites of metal-free catalysts and suggested an efficient strategy for improving the catalytic stability of such catalysts.

RESULTS AND DISCUSSION

XRD patterns of pristine and modified SWCNTs are illustrated in Figure 1a. The strong diffraction peak at 25.9° and weak peak at 43.0° were respectively assigned to the (002) and (111) reflections of the hexagonal graphitic structure of carbon nanotube.[35,36] Thermal treatment and nitrogen doping at 350 or 700 °C did not significantly change the XRD patterns, indicating the stable crystal structure of the CNTs.

Raman spectra of CNTs are displayed in Figure 1b. The characteristic D band (1319 cm^{-1}), G band (1580 cm^{-1}), and 2D band (2623 cm^{-1}) were observed. The intensity ratios of D band to G band (I_D/I_G) can be used to evaluate the structural disorder of carbon materials.[37] The I_D/I_G values of oCNT, oCNT-700, NoCNT-350, and NoCNT-700 were estimated to be 0.205, 0.212, 0.247, and 0.354, respectively. It could be found that the defective degrees of oCNT and oCNT-700 were at a low level. Also, N doping could bring about great interruption to the well-ordered sp^2-hybridized and curved honeycomb nanosheets. It was worthwhile to note that the I_D/I_G value of NoCNT was much lower than that of the doped graphene (commonly >1),[37−39] suggesting that after doping the graphitic structure of CNTs still remained very well, which could also be confirmed by the results of XRD, SEM (scanning electron microscopy), and TEM (transition electron microscopy) (Figures S1 and S2, Supporting Information).[40]

XPS studies were carried out to give insights into the composition and chemical states of nitrogen-doped CNTs. As shown in Figure 1c, 2.34 atom % of oxygen was present on the pristine CNTs due to the pretreatment using nitric acid. The oxygen levels were subsequently reduced to 1.40, 1.84, and 1.15 atom % on oCNT-700 after thermal annealing, NoCNT-350

dx.doi.org/10.1021/cs5017613 | ACS Catal. 2015, 5, 553−559

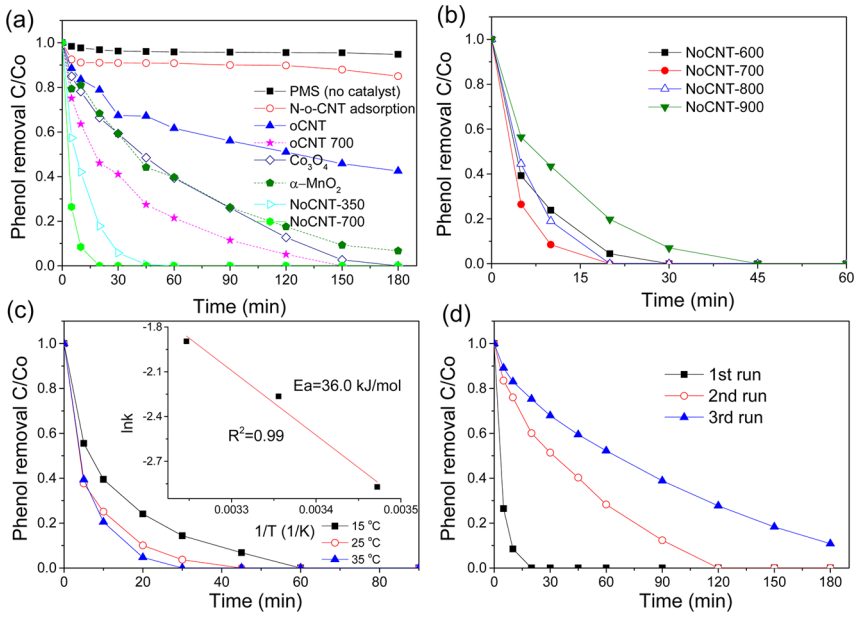

Figure 2. (a) Phenol removal under various conditions. (b) Effect of N-doping temperature on catalytic activity. (c) Effect of reaction temperature on phenol degradation and estimation of activation energy (inset) (catalyst 50 mg/L). (d) Stability tests of PMS/NoCNT-700. Reaction conditions: phenol 20 ppm, catalyst 100 mg/L, PMS 6.5 mM, temperature 25 °C.

(low-temperature doping), and NoCNT-700 (high-temperature doping), respectively. The oxygen contents in the CNT samples were much lower than those of rGO (14.44 atom %) and N-rGO (11.53 atom %) derived from reduction of graphite oxide;[27] therefore, the effect of oxygen functional groups on catalytic performance was minimized. It is well-known that oxides (carboxyl and lactone) started to decompose at elevated temperatures and the oxygen functional groups played a significant role in reacting with the nitrogen precursors to form C−N bonds in the doping process.[37,41,42] In this study, N doping at around 0.75 and 0.80 was achieved on NoCNT-350 and NoCNT-700, respectively. The relatively low doping levels in comparison with that of N-rGO (5.61 atom %)[27] was ascribed to the highly stable structure of the rolled graphene sheets, as rGO usually underwent a self-reconstruction and refabrication process during the thermal annealing and doping processes.[28,43] The high-resolution XPS N 1s spectrum of NoCNT-700 (Figure 1d) was fitted into four peaks with binding energies at 398.2, 399.9, 401.2, and 403.5 eV, corresponding to the pyridinic, pyrrolic, graphitic (or quaternary) N, and nitrogen oxides, respectively.[37,41,42] Substitutional nitrogen doping was achieved at a portion of 16.0 atom % in the overall nitrogen dopants. On the other hand, only pyridinic and pyrrolic nitrogen species were found in NoCNT-350 (Figure S5, Supporting Information) due to the low annealing temperature.[28] It was well established that a higher annealing temperature can produce more graphitic nitrogen in the carbon network.[37,42,44]

The catalytic performances of the metal-free nanocarbon materials were evaluated in catalytic activation of PMS for phenol degradation in water solutions. As shown in Figure 2a, PMS itself could barely degrade phenol, indicating that ambient temperature is not able to activate PMS to produce sulfate radicals. Without PMS, only 10% phenol was removed due to adsorption. Undoped oCNT showed a moderate activity in PMS activation, and 56.5% phenol was decomposed in 180 min with sulfate radicals. It was found that both high-temperature annealing and nitrogen doping can significantly improve the catalytic activity of CNT samples. Phenol removal at 100% was achieved on NoCNT-700, NoCNT-350, and oCNT-700 in 20, 45, and 150 min, respectively. The reaction rate constants for the oCNT, oCNT-700, and NoCNT-700 were estimated to be 0.0043, 0.0231, and 0.2466 min^{-1}, respectively, and NoCNT-700 presented 57.4- and 10.7-fold enhancement over oCNT and oCNT-700, respectively. The catalytic activities of CNT samples were compared with those of two of the most popular metal-based catalysts under the same conditions. α-MnO_2 and Co_3O_4 provided 93.3% and 100% phenol removal in 180 min, respectively, and the degradation rate of NoCNT-700 was 16.9 and 15.6 times higher than those of α-MnO_2 and Co_3O_4 accordingly, implying that the metal-free catalyst demonstrated a superior efficiency in PMS activation for phenol degradation.

Figure 2b presents the catalytic performances of N-doped CNTs derived at different annealing temperatures. It was found that the best catalytic performance was achieved on NoCNT-700. It was reported that high annealing temperature could generate more quaternary nitrogen, which is more thermally stable than the pyrrolic N, into the carbon lattice during the reconstruction of graphene sheets under annealing. However, an even higher temperature would give rise to the breakup of the C−N bond and nitrogen removal.[37,42,44] The effect of solution temperature on PMS activation on NoCNT-700 is shown in Figure 2c. It can be seen that the phenol degradation efficiency slightly increased at elevated temperatures. Specifically, 100% phenol removal was achieved in 60 min at 15 °C (catalyst 50 mg/L), and the reaction time for the same phenol removal efficiency decreased to 45 and 30 min at 25 and 35 °C, respectively. The activation energy was reduced from 43.8 kJ/mol (on oCNT-700 in Figure S9, Supporting Information) to 36.0 kJ/mol (on NoCNT-700) after nitrogen modification.

Reusability tests were also carried out on NoCNT-700 and are shown in Figure 2d. The fresh sample (first run) was able to completely decompose phenol in 20 min, and phenol removal at 100% and 89% was attained in 120 and 180 min for the

dx.doi.org/10.1021/cs5017613 | ACS Catal. 2015, 5, 553−559

second and third runs, respectively. In a similar study, MnO_2-supported cobalt catalyst decomposed 100% phenol in 90 min in the first run,[45] and the time for complete phenol removal increased to 150 and 180 min at the second and third runs, respectively. In another study,[15] the time for complete phenol oxidation on 3D MnO_2 in the first, second, and third runs was 30, 45, and 60 min, respectively. It can be seen that the catalytic activity on metal-free NoCNT-700 was not as good as that of cobalt- and manganese-based catalysts. Nevertheless, the catalytic stability of NoCNT-700 was much higher than that of rGO,[24] which achieved complete decomposition of phenol in 150 min in first run, yet only 58% and 25% phenol removal was achieved in 180 min for the second and third runs, respectively. On nitrogen-doped rGO,[27] 100% phenol removal required 45 min in the first run. However, in the second run, only 56.0% phenol removal was achieved in 180 min. The high stability of NoCNT-700 will be discussed below in a description of our mechanistic studies.

Different from the case for the polyvalent metal sites, the catalytic performance of nanocarbons in heterogeneous systems is closely related to the intricate electronic states and spin culture of the covalent carbon system.[24] PMS activation indeed relies on the electron transfer from the catalyst to PMS to break up the O_3SO-OH bond and generate active radicals. The abundant free-flowing electrons in the sp^2-hybridized graphene shell could present great potential to facilitate electron transport to HSO_5^- (PMS) to generate sulfate ($SO_4^{\bullet-}$) and hydroxyl ($^{\bullet}OH$) radicals. Unlike the flat sp^2 hybridizations of 2D graphene, the π orbitals of curved 1D carbon nanotubes contain a certain numbers of s electrons with p electrons, probably resulting in higher chemical activities.[46] In addition, defect sites such as vacancies and non-six-carbon rings, zigzag edges with unconfined π electrons, and Lewis basic groups such as ketonic and quinone groups (C═O) at the defect edges of nanocarbons played more important roles in presenting catalytic potential to induce a redox process.[21,22,24,25,47] The promoted catalytic performance of oCNT-700 was possibly due to the removal of excess surface functional groups (the oxygen contents decreased from 2.34 to 1.40 atom %), which might interfere with electron transfer from the CNT sp^2-hybridized carbon system. A decrease in oxygen content would also lead to a better reducibility of the carbon substrate, tuning the surface charge density and creating new defect sites during the thermal annealing process. Further doping of N atoms dramatically promoted the catalytic process. In a previous study, we found that nitric oxide (NO_x) demonstrated poor enhancement toward PMS activation.[28] NoCNT-350 gave a 21.4-fold enhancement over oCNT in PMS activation with a similar N doping level, yet in that case only pyridinic and pyrrolic N were formed at the defect sites other than substitutional doping in the carbon framework. NoCNT-700 successfully afforded quaternary N into the rolled graphene sheets and presented a stunning reaction rate 57.4 times faster than that of oCNT, suggesting that the graphitic N might play a key role in PMS activation. It was reported that the quaternary N has a higher electronegativity and smaller covalent radius to facilitate the electron transfer from the neighboring C, giving rise to high asymmetric spin and charge density to the adjacent carbon atoms.[44,48]

It was suggested that metal-based catalysts can activate PMS to produce both hydroxyl and sulfate radicals.[49−51] However, PMS activation processes on metal-free materials have never been investigated. Here, we first employ electron paramagnetic resonance (EPR) to probe the generation and evolution of reactive radicals using 5,5-dimethyl-1-pyrroline (DMPO) as a radical spin trapping agent. Figure 3a demonstrates that

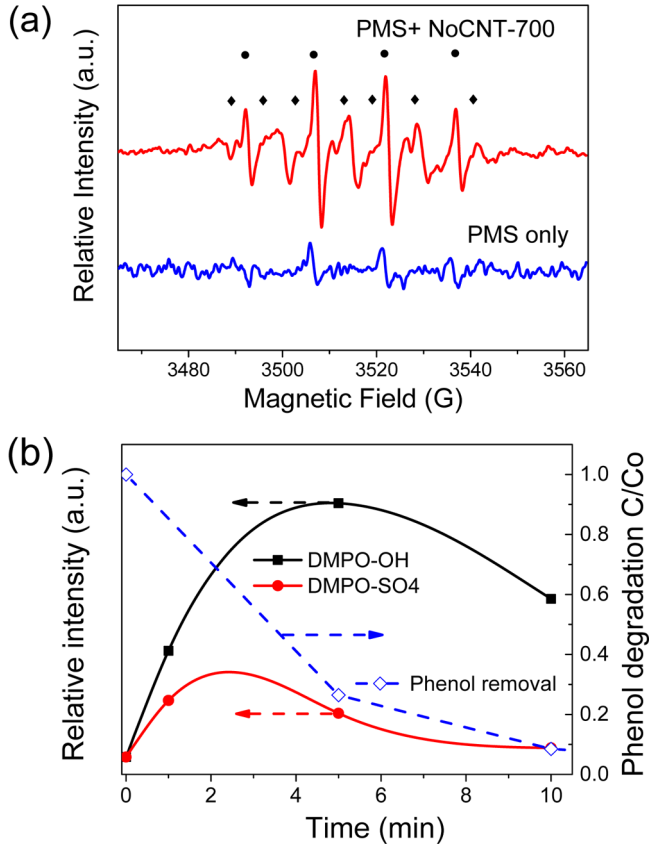

Figure 3. (a) EPR spectra of PMS activation with NoCNT-700 (●, DMPO-OH; ♦, DMPO-SO_4). (b) Radical evolution during PMS activation on NoCNT-700.

NoCNT-700 was able to effectively activate PMS to generate both $SO_4^{\bullet-}$ and $^{\bullet}OH$. Figure 3b further illustrates that the active radicals were produced rapidly, showing higher concentration in the first few minutes and then dropping gradually due to the consumption in phenol oxidation.

Ethanol was applied as a radical scavenger to quickly react with both hydroxyl and sulfate radical species ($k_{SO_4^{\bullet-}}$ = (1.6−7.8) × 10^7 M^{-1} s^{-1}, $k_{^{\bullet}OH}$ = (1.2−2.8) × 10^9 M^{-1} s^{-1}) generated in the activation process.[52] In most AOPs, the radicals are essential for the organic degradation reactions. Therefore, if the quenching reagent of ethanol is present in solution, the degradation would be significantly reduced or prevented. Control experiments were carried out to compare the catalytic performances with addition of the quenching reagent of ethanol on Co_3O_4, oCNTs, and N-doped CNTs. Figure 4a shows the effect of ethanol on phenol catalytic oxidation over a conventional catalyst of cobalt oxide. Under the standard conditions, 20 ppm of phenol was completely removed in 180 min. When ethanol was added to the reaction solution at a molar ratio of 500:1 (ethanol:PMS), phenol degradation efficiency decreased significantly. In 180 min, only around 40% of the phenol was decomposed. The more ethanol that was present in solution, the lower the phenol degradation. When all water was replaced by ethanol, no phenol degradation was observed, indicating that all generated radicals were

dx.doi.org/10.1021/cs5017613 | ACS Catal. 2015, 5, 553−559

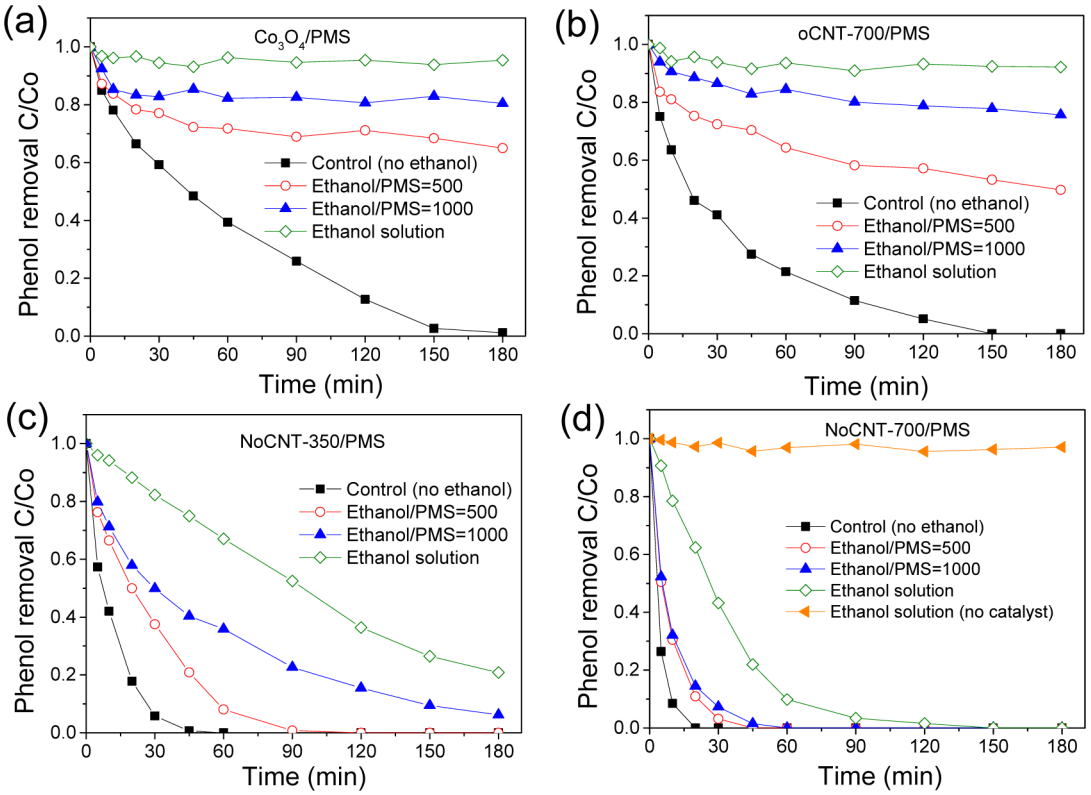

Figure 4. Effect of radical quenching on phenol degradation: (a) Co_3O_4/PMS; (b) oCNT-700/PMS; (c)NoCNT-350/PMS; (d) NoCNT-700/PMS. Reaction conditions: phenol 20 ppm, catalyst 100 mg/L, PMS 6.5 mM, temperature 25 °C.

quenched rapidly by ethanol before reacting with phenol molecules. Figure 4b examined the behavior of phenol degradation on oCNT-700 in the presence of ethanol. Results similar to those of Co_3O_4 were obtained, and no phenol degradation occurred in ethanol solution, suggesting the same degradation pathways of oCNT-700 with metal-based catalyst, Co_3O_4.

However, intrinsic differences in the quenching effects on phenol degradation were observed after heteroatom doping in CNTs. Figure 4c,d shows that NoCNT-350 and NoCNT-700 still maintained excellent phenol degradation efficiency at a high concentration of radical quenching agent with PMS. Even in ethanol solution, 79.0% and 100% phenol removal efficiencies were achieved in 180 and 150 min on NoCNT-350 and NoCNT-700, respectively. The results strongly suggested that nitrogen doping has changed the reaction mechanism and induced a new degradation pathway in metal-free NoCNT/PMS systems.

Previously, few investigations have found nonradical mechanism in Fenton-like reactions. In a previous study,[33] ceria-supported CuO was applied to the catalytic ozonation of oxalate. The oxalate degradation was dependent on neither hydroxyl radical oxidation nor acid assistance, which were common pathways in such a system. The Cu(II) formed on the catalyst surface was suggested to be an active site in coordination with oxalate and then creation of a multidentate surface complex, leading to oxalate decomposition by intramolecular electron transfer. More recently, it was reported that PDS could be activated by CuO via a nonradical process through outer-sphere interaction, followed by a rapid reaction with the model compound 2,4-dichlorophenol (2,4-DCP).[34]

In this investigation, a nonradical process of phenol degradation was found to occur upon N doping in CNTs. The nonradical processes observed in CuO catalysis can be a plausible pathway for phenol degradation on nitrogen-doped CNT samples. In the nonradical process, the oxidant (PMS) would be first bonded with the sp^2-hybridized system and then react with the adsorbed phenol molecules as shown in Scheme 1. The highly covalent π electrons could activate the O−O bond in PMS, and nitrogen dopants (especially for the quaternary N) would further activate the adjacent carbons and dramatically enhance the catalytic performance.

Interestingly, it was found that the effect of reaction temperature on NoCNT catalysis was not as significant as

Scheme 1. Mechanism of PMS Activation on N-Doped CNTs

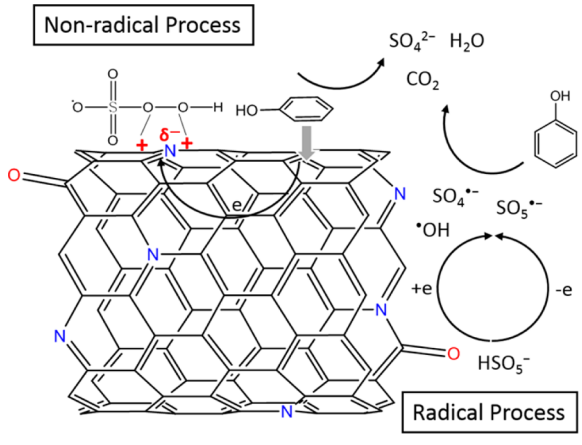

dx.doi.org/10.1021/cs5017613 | ACS Catal. 2015, 5, 553−559

PMS activation on the undoped oCNT-700 and metal-based catalysts. The same phenomenon was also reported in the N-MWCNT[28] and nitrogen=modified graphene (Figure S9, Supporting Information). Nitrogen heteroatoms in CNT might greatly enhance both the radical and nonradical pathways, which gave rise to a more significant effect than the reaction temperature that controls the electron transfer in the typical radical generation processes. Accordingly, the enhanced catalytic performance can be ascribed to both radical and nonradical processes, which were significantly promoted by nitrogen doping. In addition, it is worth noting that the stability of NoCNT samples was much better than that of rGO and N-doped graphene in our previous studies.[24,27] It was deduced that the defect sites at the carbon edges and functional groups, which played a crucial role in the radical generation, might be covered by the adsorbed phenol and intermediates during the reaction (Figure S11, Supporting Information).[27] The deactivation process was ascribed to modulation of the charge distribution and functional groups on CNT surface and reconstruction of the dopants (Figure S12, Supporting Information). As the carbon structure in the curved graphene shell of CNT was much more stable, it was more difficult to change the structure and surface chemistry of the rolled CNT in comparison to changing the chemically derived graphene sheets. Since the nonradical processes mainly rely on the activated sp^2 carbon network which was induced by the substantial N doping, the N-doped carbon nanotubes retain high activity and stability in reuses.

CONCLUSIONS

In conclusion, the chemical modification of SWCNTs with substitutional N incorporation into the rolled graphene sheets was achieved. NoCNT-700 presented an extraordinarily high catalytic activity for phenol removal by PMS activation with a 57.4-fold enhancement over the activity of oCNT, as well as 16.9- and 15.6-fold enhancement over the activity of the most effective metal catalysts, α-MnO_2 and Co_3O_4, respectively. The mechanism of PMS activation on carbon nanotubes was illustrated. For the first time, we discovered that both radical and nonradical pathways contribute to the phenol degradation on NoCNT with PMS activation. Among the N dopants, graphitic N plays a key role in the nonradical-based oxidation process. It was also found that the temperature slightly affects the catalytic efficiency after nitrogen modification and the as-prepared catalysts presented a much better stability for reuse. Since the nitrogen doping level is low in this work, future studies may be required to investigate the effect of nitrogen doping levels on the enhanced catalytic performance and reusability. This study provided insights into the roles of nitrogen heteroatoms of nanocarbons for enhanced catalysis and, more importantly, presented a novel view for improving the reusability of metal-free catalysts.

EXPERIMENTAL SECTION

Synthesis of Nitrogen-Modified Single-Walled Carbon Nanotubes (SWCNTs). Commercial SWCNTs (1.0 g, 99.9%) were first mixed with nitric acid (100 mL, 70 wt %) and the mixtures stirred on a hot plate at 100 °C for 4 h to remove any metal residuals to give metal-free CNT (oCNT). The material was filtered and washed with ultrapure water and dried in an oven at 60 °C overnight. Melamine was added to the oCNT/ethanol suspension, and this mixture was stirred at 50 °C to evaporate ethanol to give a homogeneous mixture of oCNT and melamine. The dried mixture was transferred to a tube furnace for annealing at 700 °C for 1 h under an N_2 (40 mL/min) atmosphere. The sample was collected and washed with ultrapure water several times and dried at 60 °C in an oven overnight. Thus, nitrogen-doped carbon nanotubes (NoCNT-700) were obtained. oCNT-700 was prepared with the same procedure without melamine. NoCNT-350 was prepared using ammonium nitrate as a N precursor for annealing at 350 °C.

Characterization of Materials. X-ray diffraction (XRD) patterns were obtained on a Bruker D8-Advanced X-ray instrument using Cu Kα radiation with λ 1.5418 Å. Raman spectra were acquired on an ISA dispersive Raman spectrometer using argon ion lasers (514 nm). X-ray photoelectron spectroscopy (XPS) was performed on a Kratos AXIS Ultra DLD system under UHV conditions with Al Kα X-ray to investigate the composition and chemical states. Data were analyzed with Kratos Vision and CasaXPS software.

Evaluation of the Catalytic Performance. The catalytic activity of the materials was evaluated in the catalytic oxidation of phenol. The reactions were carried out in phenol aqueous solution (20 ppm, 500 mL) with a catalyst (100 mg/L) and PMS (6.5 mM) at 25 °C. During each interval, 1 mL of the solution was withdrawn by a syringe, filtered by a 0.45 μm film, and injected into a vial that was previously filled with 0.5 mL of methanol for quenching the reaction. The sample was analyzed by high-performance liquid chromatography (HPLC, Varian) with a C-18 column. After each run, the used catalyst was collected by ultrasonic washing for 5 min and washed three times with ultrapure water (500 mL), filtered, and dried in an oven for reuse.

Mechanistic Studies of the Catalytic Processes. An EMS-plus EPR instrument from Bruker was employed to detect the free radicals captured by 5,5-dimethyl-1-pyrroline (DMPO, >99.0%) during PMS activation, operating under the following conditions: center field, 3515 G; sweep width, 100 G; microwave frequency, 9.87 GHz; power setting, 18.75 mW; scan number, 3. The radical quantitative information was acquired from the Spin Fitting from Bruker Xenon Software Package. Identification of major radicals as well as the radical vs nonradical processes were investigated by classical quenching tests. The procedure was similar to the typical phenol degradation mentioned above, but the reactions were carried out with addition of different amounts of ethanol.

ASSOCIATED CONTENT

Supporting Information

The following file is available free of charge on the ACS Publications website at DOI: 10.1021/cs5017613.

Preparation procedures of nanocrystalline Co_3O_4 and MnO_2, XPS survey, phenol oxidation on various nanocarbons, and TOC, FTIR and EPR spectra (PDF)

AUTHOR INFORMATION

Corresponding Authors

*H.S.: e-mail, h.sun@curtin.edu.au; tel, +61 8 9266 9211.
*S.W.: e-mail, shaobin.wang@curtin.edu.au; tel, +61 8 9266 3776.

Notes

The authors declare no competing financial interest.

■ ACKNOWLEDGMENTS

This work was financially supported by the Australian Research Council (DP130101319). The authors acknowledge the use of equipment and scientific and technical assistance of the Electron Microscope Facility, which has been partially funded by the University, State, and Commonwealth Governments, and the WA X-ray Surface Analysis Facility, funded by the Australian Research Council LIEF grant (LE120100026). H.S. is grateful for support from the Curtin Research Fellowship.

■ REFERENCES

(1) Behrens, M.; Studt, F.; Kasatkin, I.; Kuhl, S.; Havecker, M.; Abild-Pedersen, F.; Zander, S.; Girgsdies, F.; Kurr, P.; Kniep, B. L.; Tovar, M.; Fischer, R. W.; Norskov, J. K.; Schlogl, R. *Science* **2012**, *336*, 893−897.
(2) Chen, M. S.; Kumar, D.; Yi, C. W.; Goodman, D. W. *Science* **2005**, *310*, 291−293.
(3) Liu, S. W.; Yu, J. G.; Jaroniec, M. *J. Am. Chem. Soc.* **2010**, *132*, 11914−11916.
(4) Ishikawa, A.; Takata, T.; Kondo, J. N.; Hara, M.; Kobayashi, H.; Domen, K. *J. Am. Chem. Soc.* **2002**, *124*, 13547−13553.
(5) Saputra, E.; Muhammad, S.; Sun, H. Q.; Ang, H. M.; Tade, M. O.; Wang, S. B. *Appl. Catal., B* **2013**, *142*, 729−735.
(6) Montoya, J. F.; Bahnemann, D. W.; Peral, J.; Salvador, P. *ChemPhysChem* **2014**, *15*, 2311−2320.
(7) Besson, M.; Gallezot, P. *Catal. Today* **2000**, *57*, 127−141.
(8) Zhang, J. A.; Su, D. S.; Blume, R.; Schlogl, R.; Wang, R.; Yang, X. G.; Gajovic, A. *Angew. Chem., Int. Ed.* **2010**, *49*, 8640−8644.
(9) Andreozzi, R.; Caprio, V.; Insola, A.; Marotta, R. *Catal. Today* **1999**, *53*, 51−59.
(10) Zazo, J. A.; Casas, J. A.; Mohedano, A. F.; Gilarranz, M. A.; Rodriguez, J. J. *Environ. Sci. Technol.* **2005**, *39*, 9295−9302.
(11) Yang, L.; Hu, C.; Nie, Y. L.; Qu, J. H. *Environ. Sci. Technol.* **2009**, *43*, 2525−2529.
(12) Zhao, W.; Ma, W. H.; Chen, C. C.; Zhao, J. C.; Shuai, Z. G. *J. Am. Chem. Soc.* **2004**, *126*, 4782−4783.
(13) Anipsitakis, G. P.; Dionysiou, D. D.; Gonzalez, M. A. *Environ. Sci. Technol.* **2006**, *40*, 1000−1007.
(14) Anipsitakis, G. P.; Dionysiou, D. D. *Environ. Sci. Technol.* **2004**, *38*, 3705−3712.
(15) Wang, Y.; Sun, H.; Ang, H. M.; Tadé, M. O.; Wang, S. *Appl. Catal., B* **2015**, *164*, 159−167.
(16) Ball, D. L.; Edwards, J. O. *J. Am. Chem. Soc.* **1956**, *78*, 1125−1129.
(17) Buxton, G. V.; Greenstock, C. L.; Helman, W. P.; Ross, A. B. *J. Phys. Chem. Ref. Data* **1988**, *17*, 513−886.
(18) Neta, P.; Huie, R. E.; Ross, A. B. *J. Phys. Chem. Ref. Data* **1988**, *17*, 1027−1284.
(19) Saputra, E.; Muhammad, S.; Sun, H. Q.; Ang, H. M.; Tade, M. O.; Wang, S. B. *Environ. Sci. Technol.* **2013**, *47*, 5882−5887.
(20) Anipsitakis, G. P.; Stathatos, E.; Dionysiou, D. D. *J. Phys. Chem. B* **2005**, *109*, 13052−13055.
(21) Frank, B.; Blume, R.; Rinaldi, A.; Trunschke, A.; Schlogl, R. *Angew. Chem., Int. Ed.* **2011**, *50*, 10226−10230.
(22) Frank, B.; Zhang, J.; Blume, R.; Schlogl, R.; Su, D. S. *Angew. Chem., Int. Ed.* **2009**, *48*, 6913−6917.
(23) Zhang, J.; Liu, X.; Blume, R.; Zhang, A. H.; Schlogl, R.; Su, D. S. *Science* **2008**, *322*, 73−77.
(24) Sun, H. Q.; Liu, S. Z.; Zhou, G. L.; Ang, H. M.; Tade, M. O.; Wang, S. B. *ACS Appl. Mater. Interfaces* **2012**, *4*, 5466−5471.
(25) Liu, S. Z.; Peng, W. C.; Sun, H. Q.; Wang, S. B. *Nanoscale* **2014**, *6*, 766−771.
(26) Peng, W. C.; Liu, S. Z.; Sun, H. Q.; Yao, Y. J.; Zhi, L. J.; Wang, S. B. *J. Mater. Chem. A* **2013**, *1*, 5854−5859.
(27) Sun, H. Q.; Wang, Y. X.; Liu, S. Z.; Ge, L.; Wang, L.; Zhu, Z. H.; Wang, S. B. *Chem. Commun.* **2013**, *49*, 9914−9916.
(28) Sun, H. Q.; Kwan, C.; Suvorova, A.; Ang, H. M.; Tade, M. O.; Wang, S. B. *Appl. Catal., B* **2014**, *154*, 134−141.
(29) Bepete, G.; Tetana, Z. N.; Lindner, S.; Rummeli, M. H.; Chiguvare, Z.; Coville, N. J. *Carbon* **2013**, *52*, 316−325.
(30) Shi, F.; Tse, M. K.; Li, Z. P.; Beller, M. *Chem. Eur. J.* **2008**, *14*, 8793−8797.
(31) Deguillaume, L.; Leriche, M.; Chaurnerliac, N. *Chemosphere* **2005**, *60*, 718−724.
(32) Nunes, G. S.; Alexiou, A. D. P.; Toma, H. E. *J. Catal.* **2008**, *260*, 188−192.
(33) Zhang, T.; Li, W. W.; Croue, J. P. *Appl. Catal., B* **2012**, *121*, 88−94.
(34) Zhang, T.; Chen, Y.; Wang, Y.; Le Roux, J.; Yang, Y.; Croué, J.-P. *Environ. Sci. Technol.* **2014**, *48*, 5868−5875.
(35) Zhao, A. Q.; Masa, J.; Xia, W.; Maljusch, A.; Willinger, M. G.; Clavel, G.; Xie, K. P.; Schlogl, R.; Schuhmann, W.; Muhlert, M. *J. Am. Chem. Soc.* **2014**, *136*, 7551−7554.
(36) Chen, P. R.; Yang, F. K.; Kostka, A.; Xia, W. *ACS Catal.* **2014**, *4*, 1478−1486.
(37) Long, J. L.; Xie, X. Q.; Xu, J.; Gu, Q.; Chen, L. M.; Wang, X. X. *ACS Catal.* **2012**, *2*, 622−631.
(38) Wang, S. Y.; Zhang, L. P.; Xia, Z. H.; Roy, A.; Chang, D. W.; Baek, J. B.; Dai, L. M. *Angew. Chem., Int. Ed.* **2012**, *51*, 4209−4212.
(39) Zheng, Y.; Jiao, Y.; Ge, L.; Jaroniec, M.; Qiao, S. Z. *Angew. Chem., Int. Ed.* **2013**, *52*, 3110−3116.
(40) Higgins, D. C.; Hoque, M. A.; Hassan, F.; Choi, J.-Y.; Kim, B.; Chen, Z. *ACS Catal.* **2014**, *4*, 2734−2740.
(41) Sheng, Z. H.; Shao, L.; Chen, J. J.; Bao, W. J.; Wang, F. B.; Xia, X. H. *ACS Nano* **2011**, *5*, 4350−4358.
(42) Li, X. L.; Wang, H. L.; Robinson, J. T.; Sanchez, H.; Diankov, G.; Dai, H. J. *J. Am. Chem. Soc.* **2009**, *131*, 15939−15944.
(43) Yang, Z.; Yao, Z.; Li, G. F.; Fang, G. Y.; Nie, H. G.; Liu, Z.; Zhou, X. M.; Chen, X.; Huang, S. M. *ACS Nano* **2012**, *6*, 205−211.
(44) Deng, D. H.; Pan, X. L.; Yu, L. A.; Cui, Y.; Jiang, Y. P.; Qi, J.; Li, W. X.; Fu, Q. A.; Ma, X. C.; Xue, Q. K.; Sun, G. Q.; Bao, X. H. *Chem. Mater.* **2011**, *23*, 1188−1193.
(45) Liang, H. W.; Sun, H. Q.; Patel, A.; Shukla, P.; Zhu, Z. H.; Wang, S. B. *Appl. Catal., B* **2012**, *127*, 330−335.
(46) Kong, X. K.; Chen, C. L.; Chen, Q. W. *Chem. Soc. Rev.* **2014**, *43*, 2841−2857.
(47) Jiang, D. E.; Sumpter, B. G.; Dai, S. *J. Chem. Phys.* **2007**, *126*, No. 134701.
(48) Zhao, Y.; Yang, L. J.; Chen, S.; Wang, X. Z.; Ma, Y. W.; Wu, Q.; Jiang, Y. F.; Qian, W. J.; Hu, Z. *J. Am. Chem. Soc.* **2013**, *135*, 1201−1204.
(49) Bennett, J. E.; Gilbert, B. C.; Stell, J. K. *J. Chem. Soc, Perkin Trans 2* **1991**, 1105−1110.
(50) Gilbert, B. C.; Stell, J. K. *J. Chem. Soc, Perkin Trans 2* **1990**, 1281−1288.
(51) Gilbert, B. C.; Stell, J. K. *J. Chem. Soc, Faraday Trans* **1990**, *86*, 3261−3266.
(52) Anipsitakis, G. P.; Dionysiou, D. D. *Environ. Sci. Technol.* **2003**, *37*, 4790−4797.